12-2-2013

Homogeneous AlGaN/GaN superlattices grown on free-standing (1(1)over-bar00) GaN substrates by plasma-assisted molecular beam epitaxy

Jiayi Shao
Purdue University, Birck Nanotechnology Center, shao20@purdue.edu

Dmitri N. Zakharov
Purdue University, Birck Nanotechnology Center, zakharov@purdue.edu

Collin Edmunds
Purdue University, cedmunds@purdue.edu

Oana Malis
Purdue University, Birck Nanotechnology Center, omalis@purdue.edu

Michael J. Manfra
Purdue University, Brick Nanotechnology Center, mmanfra@purdue.edu

AIP | Applied Physics Letters

Homogeneous AlGaN/GaN superlattices grown on free-standing (1 1 ¯ 00) GaN substrates by plasma-assisted molecular beam epitaxy

Jiayi Shao, Dmitri N. Zakharov, Colin Edmunds, Oana Malis, and Michael J. Manfra

Citation: Applied Physics Letters **103**, 232103 (2013); doi: 10.1063/1.4836975
View online: http://dx.doi.org/10.1063/1.4836975
View Table of Contents: http://scitation.aip.org/content/aip/journal/apl/103/23?ver=pdfcov
Published by the AIP Publishing

Homogeneous AlGaN/GaN superlattices grown on free-standing (1$\bar{1}$00) GaN substrates by plasma-assisted molecular beam epitaxy

Jiayi Shao,[1,2] Dmitri N. Zakharov,[3] Colin Edmunds,[2] Oana Malis,[1,2] and Michael J. Manfra[1,2,4,5]
[1]*Birck Nanotechnology Center, Purdue University, West Lafayette, Indiana 47907, USA*
[2]*Physics Department, Purdue University, West Lafayette, Indiana 47907, USA*
[3]*Center for Functional Nanomaterials, Brookhaven National Laboratory, Upton, New York 11973, USA*
[4]*School of Materials Engineering, Purdue University, West Lafayette, Indiana 49707, USA*
[5]*School of Electrical and Computer Engineering, Purdue University, West Lafayette, Indiana 49707, USA*

(Received 18 September 2013; accepted 15 November 2013; published online 3 December 2013)

Two-dimensional and homogeneous growth of m-plane AlGaN by plasma-assisted molecular beam epitaxy has been realized on free-standing (1$\bar{1}$00) GaN substrates by implementing high metal-to-nitrogen (III/N) flux ratio. AlN island nucleation, often reported for m-plane AlGaN under nitrogen-rich growth conditions, is suppressed at high III/N flux ratio, highlighting the important role of growth kinetics for adatom incorporation. The homogeneity and microstructure of m-plane AlGaN/GaN superlattices are assessed via a combination of scanning transmission electron microscopy and high resolution transmission electron microscopy (TEM). The predominant defects identified in dark field TEM characterization are short basal plane stacking faults (SFs) bounded by either Frank-Shockley or Frank partial dislocations. In particular, the linear density of SFs is approximately 5×10^{-5} cm^{-1}, and the length of SFs is less than 15 nm. © *2013 AIP Publishing LLC*. [http://dx.doi.org/10.1063/1.4836975]

While non-polar III-Nitride heterostructures show great promise in many optoelectronic and electronic devices due to the lack of spontaneous polarization and piezoelectric polarization fields,[1–5] it remains a challenge to obtain high quality (1$\bar{1}$00) m-plane AlGaN/GaN superlattices with smooth interfaces and low defect density.[6] Heteroepitaxy of non-polar nitride-based heterostructures on foreign substrates via molecular beam epitaxy (MBE) and metalorganic chemical vapor deposition (MOCVD) is strongly hampered by the high density of dislocations and stacking faults (SFs). Growth on free-standing m-plane (1$\bar{1}$00) GaN substrates with low defect density presents an attractive path forward. Epitaxial growth of non-polar and semi-polar nitride-based materials produced by MOCVD is well documented.[11–20] However, there have been relatively few reports of m-plane (1$\bar{1}$00) AlGaN/GaN heterostructures grown by MBE;[7–10] most have focused on issues related to anisotropy occurring under nitrogen-rich growth conditions. Hoshi *et al.*[8] discussed crystal mosaicity and luminescence spectra in AlGaN films grown on GaN by MBE using NH_3 as a nitrogen source. Young *et al.*[9] reported on cracking and anisotropic lattice relaxation in AlGaN films also grown by ammonia MBE on GaN substrates. Ammonia MBE growth typically is realized with a low III/N ratio, i.e., under nitrogen-rich conditions. Transmission electron microscopy (TEM) characterization of the resulting microstructure was not reported in Refs. 8 and 9. Smalc-Koziorowska *et al.*[10] reported plasma-assisted MBE (PAMBE) growth under nitrogen-rich conditions of (1$\bar{1}$00) m-plane AlGaN/GaN superlattice on free-standing m-plane GaN substrates in which pure AlN islands (150–400 nm long) are formed by a growth induced relaxation mechanism resulting in stacking faults formation in the (0001) plane. At this time, growth of AlGaN/GaN m-plane superlattices utilizing a broader range of PAMBE growth conditions (e.g., gallium to nitrogen flux ratio) and the microstructure generated under these growth conditions requires investigation.

In this Letter, we demonstrate that chemically homogeneous and high quality m-plane AlGaN/GaN superlattices can be grown by PAMBE with Ga/N ratio $\geq$1 on free-standing m-plane substrates. Atomic step flow surface morphologies were observed with atomic force microscopy (AFM). Well-formed and homogeneous superlattices with sharp interfaces are evident from high resolution x-ray diffraction (HRXRD) analysis and scanning transmission electron microscopy (STEM). With Ga/N $\geq$1, no evidence of the formation of AlN islands within the AlGaN barriers reported in Ref. 10 is found, suggesting that growth kinetics plays an important role for alloy homogeneity and strain relaxation. Defect formation in m-plane AlGaN/GaN superlattices grown under high III/N ratio has been studied using dark-field TEM characterization. The predominant defects are short basal plane (BP) SFs bounded by Frank-Shockley or Frank partial dislocations. The linear defect density of SFs is approximately 5×10^{-5} cm^{-1}, and the length of SFs is in the range of 2–15 nm.

Our free-standing m-plane substrates[21] have rectangular shape (approximately 10 mm by 5 mm) and are cut from few-millimeter thick free-standing crystals grown by hydride vapor phase epitaxy in the c-direction. The nominal threading dislocation density is $\sim 5 \times 10^6$ cm^{-2}. As received, the substrates are smooth with typical root-mean-square (rms) roughness of 0.2–0.3 nm over 16 μm^2. We have grown two superlattices (sample A and sample B) to study the impact of high III/N ratio during MBE growth. Both AlGaN/GaN superlattices were grown under metal-rich conditions with $1.0 \leq$ Ga/N ≤ 1.2. Sample A is grown on an m-plane substrate miscut towards [000$\bar{1}$] by 0.2°, while sample B is

grown on a substrate miscut towards [0001] by 0.4°. Sample A consists of a 10 nm/16.7 nm $Al_{0.1}Ga_{0.9}N$/GaN superlattice structure with 10 repeats, while sample B consists of a 3.1 nm/9.8 nm $Al_{0.17}Ga_{0.83}N$/GaN superlattice structure with 50 repeats. Gallium flux was supplied by a conventional effusion cell, and nitrogen flux was provided by a Veeco Unibulb radio-frequency plasma source operating at 300W forward power with 0.5 sccm of nitrogen (N_2) flow. The substrate temperature is monitored with a pyrometer: 720 °C for sample A and 740 °C for sample B. The growth rates of both AlGaN and GaN are 7 nm/min under these conditions.

After growth, the surface morphologies were measured by AFM in tapping mode, and the rms roughness was measured. Insets of Figures 1(a) and 1(b) indicate smooth surface morphologies with visible atomic steps in both sample A and B. In a previous work,[21] we demonstrated that atomically smooth morphology is produced for m-plane GaN growth under high III/N ratio on substrates miscut towards both ±c-directions with proper choice of substrate temperature. This feature is also seen in the AlGaN/GaN superlattices. The rms roughness over 1 μm^2 is 0.37 nm and 0.10 nm in samples A and B, respectively. No island-like features are observed in AFM, and the terrace widths observed are consistent with the quoted miscut angles. Although both substrates are nominally miscut towards ±c-direction, the terrace direction in Figure 1(a) may indicate a slight accidental miscut towards [11$\bar{2}$0]. Figures 1(a) and 1(b) show HRXRD $\omega/2\theta$ scans of the (1$\bar{1}$00) axis reflection of these two samples. Data were collected using a PANalytical X'Pert-MRD high-resolution x-ray diffractometer equipped with a four-bounce Ge monochromator. Satellite peaks were observed confirming the existence of the superlattice structure. The pendellösung fringes and narrow superlattice satellite peaks are indicative of abrupt interfaces between AlGaN and GaN layers and layer uniformity. Simulation of the diffraction pattern using the commercial software package PANalytical X'PERT EPITAXY enabled estimation of well and barrier thicknesses as well as the aluminum composition. The aluminum compositions were obtained by simulation of the HRXRD pattern using accurate barrier and well thicknesses determined with STEM characterization as shown in Figure 2. The Al composition is 10% in sample A and 17% in sample B.

Conventional dark field (DF) TEM imaging was performed on a JEOL 2100F operated at 200 kV. High resolution TEM (HRTEM) imaging was done on an aberration-corrected FEI Titan 80–300 electron microscope operated at 300 kV. Scanning transmission electron microscopy observations were performed on a Hitachi HD 2700C STEM operated at 200 kV.

Low magnification and high resolution high-angle annular dark field (HAADF) STEM images of samples A and B are shown in Figure 2. The AlGaN layers appear darker than the surrounding GaN layer due to the lower average atomic

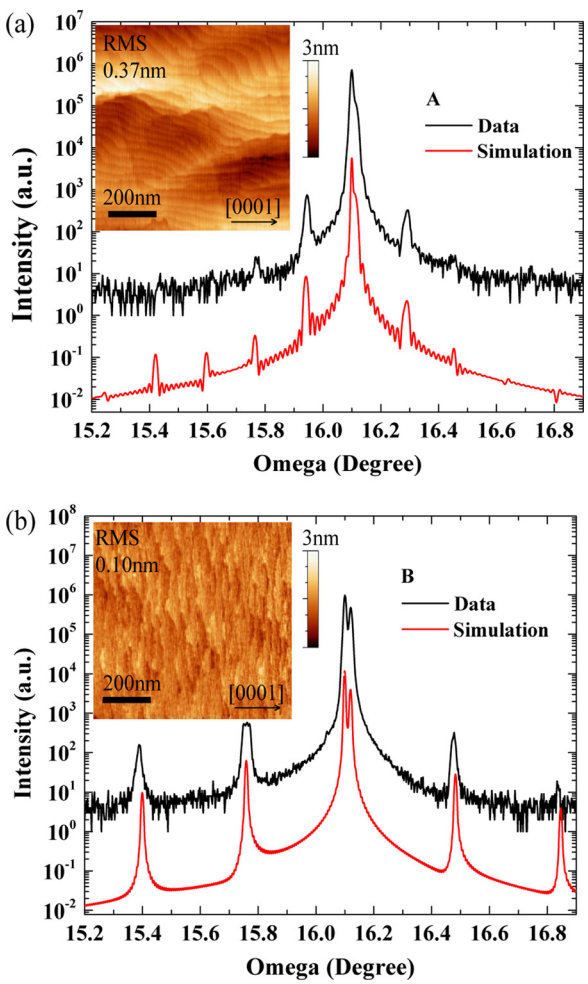

FIG. 1. HRXRD $\omega/2\theta$ scans of the (1$\bar{1}$00) reflection: Fig. 1(a) sample A and Fig. 1(b) sample B. Insets: surface morphology measured with AFM.

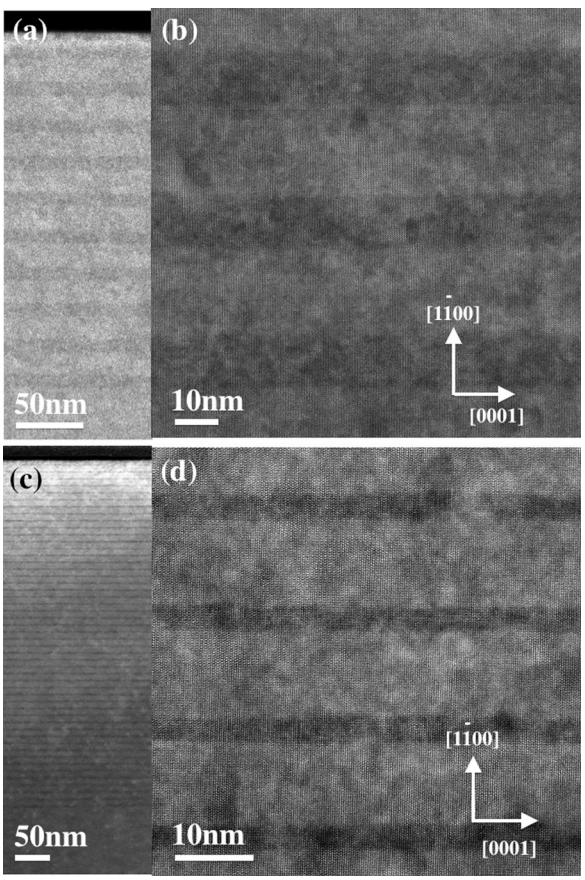

FIG. 2. HAADF STEM images taken along the [11$\bar{2}$0] zone axis (a) low magnification image of sample A, (b) high resolution image of sample A, (c) low magnification image of sample B, (d) high resolution image of sample B

number. These images indicate AlGaN barrier thickness of 10 nm and GaN well thickness of 16.7 nm in sample A, and barrier thickness of 3.1 nm and well thickness of 9.8 nm in sample B. For both samples, each individual layer thickness is uniform along the lateral direction, and there are abrupt interfaces between AlGaN and GaN layers in high-resolution images. This is in good agreement with pendellösung fringes and narrow superlattice satellite peaks measured via HRXRD. Despite extensive searching, we do not find any indication of AlN island inclusions in either superlattice (10% or 17% AlGaN) as observed in Ref. 10. This is a central finding of our work.

A complete theoretical understanding of the mechanisms driving adatom segregation and AlN inclusion formation on m-plane is currently lacking. In Ref. 10, the mechanism driving metal atom segregation and the formation of AlN inclusions is not identified. We ascribe the difference in microstructure seen in our work to the very different Ga/N ratio used as compared to Ref. 10. High Ga/N ≥ 1 used here appears to favor more homogeneous aluminum incorporation. Wang *et al.*[22] reported that a gallium wetting layer on the surface of a growing c-plane nitride film is not only highly mobile itself but also increases mobility of other species present in the wetting layer. It is conceivable that the same mechanism could be active for low aluminum composition AlGaN grown by PAMBE on m-plane substrates as well, providing better homogeneity in AlGaN layers grown under metal-rich conditions. Calculations by Lymperakis[27] and Neugebauer indicate anisotropic adatom diffusion barriers along the c- and a-axes for m-plane GaN, resulting in the often observed "slate-like" growth morphology. Our previous work[21] indicates that this effect can be mitigated at high Ga/N ratio, producing atomically smooth step flow morphology. As discussed by Albrecht *et al.*[25] for c-plane growth, adatom incorporation in AlGaN depends in a complicated manner on a number of factors including surface bond configuration, accessible vicinal facets, and adatom diffusion. In Ref. 10, strain-driven segregation was suggested as a possible mechanism to explain the observed inclusions. Our results indicate that adatom surface mobility must play an equally important role in the formation of homogeneous alloys on the $(1\bar{1}00)$ surface. Bourret,[26] in particular, stressed the importance platelet formation during the initial stages of c-plane AlN growth on GaN and determined that platelet coalescence and dislocation introduction are very dependent on the III/N ratio. Nitrogen-rich growth conditions enhance the formation of stacking faults and dislocation nucleation.[26] It is conceivable that similar physics drives the differences between our results and those of Ref. 10 for m-plane AlGaN growth but more work is needed. It is also noteworthy that, despite some differences in surface morphology, homogeneous AlGaN is grown on wafers slightly miscut towards both ±c-directions, so long as III/N > 1 conditions are used.

In order to precisely characterize the defect structure generated under our high III/N ratio growth conditions, DF TEM was implemented to study the defect distribution within the superlattices. Figures 3(a) and 3(c) represent DF TEM images of sample A and B taken close to the $[11\bar{2}0]$ zone axis with strongly excited vector $\boldsymbol{g} = 1\bar{1}00$. For this imaging condition, stacking faults formed in the basal plane of wurtzite GaN structure are in strong contrast. Some basal plane stacking faults are marked with black arrows in Figures 3(a) and 3(c). From residual contrast of AlGaN/GaN layers in Figure 3(c), one can notice random distribution of BP-SFs across the layers. While some defects nucleate in a GaN layer and then terminate in the next AlGaN layer or vice versa, others start in a GaN layer, pass through the AlGaN layer and terminate in the next GaN layer. Dislocations terminating BP-SFs are in strong contrast for two beam conditions with strongly excited vector $\boldsymbol{g} = 0002$. They are marked with white arrows in Figures 3(b) and 3(d). Densities of dislocations measured from two beam condition images in Figures 3(b) and 3(d) equal 6.7×10^{11} cm^{-2} and 3.7×10^{11} cm^{-2} for samples A and B, respectively. BP-SF lengths for sample A vary from 2.2 nm to 5.5 nm. For sample B, the length varies between 2.2 nm and 15.2 nm. In order to calculate linear densities of SFs in our samples, we utilized geometric techniques described in Ref. 23. The corresponding calculated linear densities are 7.7×10^5 cm^{-1} and 4.5×10^5 cm^{-1} for sample A and sample B, respectively. The linear density and length of SFs were not reported in Ref. 10, precluding a direct comparison, although they did report the observation of both intrinsic and extrinsic BP-SFs which allow the AlN inclusions to relax along the [0001] interface.

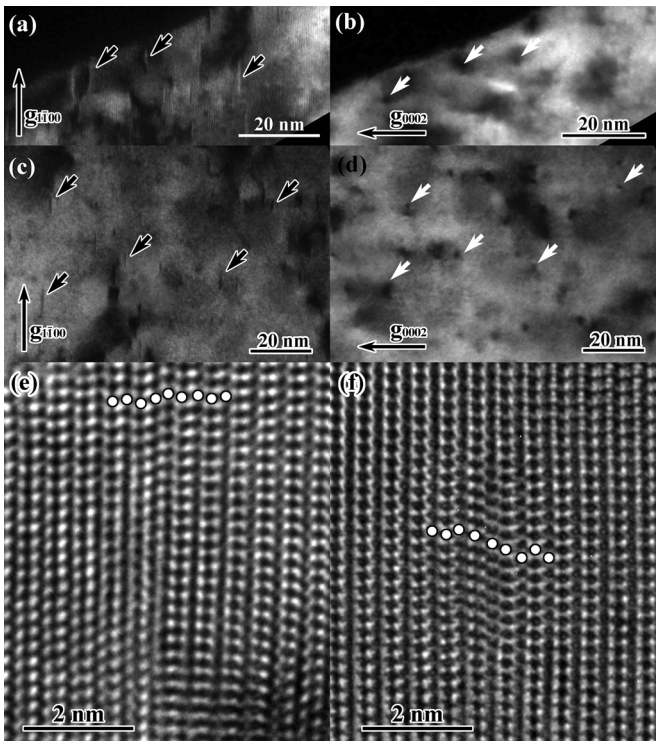

FIG. 3. (a)–(d) Dark field TEM images taken under two beam condition close to $[11\bar{2}0]$ zone axis. (a) and (b) Dark field images of sample A taken with strongly excited $g = 1\bar{1}00$ to reveal BP-SFs and $g = 0002$ to reveal PDs, respectively. (c) and (d) Dark field images of sample B taken with strongly excited (c) $g = 1\bar{1}00$ and (d) $g = 0002$. (e) and (f) High-resolution TEM images show BP-SFs with stacking sequence (e)…ABABCBCBC… (sample A) and (f)…ABABCABAB… (sample B), respectively. Corresponding stacking sequences are marked by white dots.

HRTEM revealed two major types of BP-SFs present in our superlattices, I_1 SFs and extrinsic (E-type) SFs. Figure 3(e) shows an I_1 type SF from sample A with stacking

sequence…AB**ABC**BCBC… (Faulted structure shown in bold and also marked by white dots in the image) terminated by a Frank-Shockley partial dislocation (FS-PD) with Burgers vectors $\boldsymbol{b} = 1/6\langle 2\bar{2}03\rangle$.[24] Figure 3(f) shows an extrinsic (E-type) BP-SF from sample B with stacking sequence…AB**ABC**A**B**AB….that forms a dislocation loop with Burgers vector $\boldsymbol{b} = 1/2\langle 0001\rangle$. Our results offer interesting comparison to the more heavily studied defect structure of compressively strained InGaN/GaN quantum wells used in light-emitting diodes and laser structures. In Ref. 28, generation of BP-SFs was observed in InGaN/GaN quantum wells for well thickness above 3 nm. The lateral extent parallel to the $[11\bar{2}0]$ direction was ~100 nm, significantly longer that those observed in our AlGaN/GaN superlattices. These authors also determined that the BP-SFs in their InGaN/GaN quantum wells were primarily type I_1. No E-type BP-SFs were found based in Ref. 28, whereas E-type BP-SFs are observed in our AlGaN layers under tensile strain. Further work is needed to fully understand the mechanisms of tensile strain relaxation on the m-plane of GaN.

In conclusion, using free-standing m-plane GaN substrates, m-plane AlGaN/GaN superlattices with atomically smooth surface morphologies and abrupt interfaces were produced by PAMBE with $Ga/N \geq 1$, where AlGaN growth is two-dimensional and largely isotropic. Under these conditions AlN island formation is suppressed. The predominant defects identified in dark field TEM are short BP-SFs bounded by FS-PDs. In particular, the linear defect density of SFs is approximately $5 \times 10^5\,cm^{-1}$, and the length of SFs is less than 15 nm. Production of homogeneous m-plane AlGaN/GaN superlattices as described here provides the possibility to realize the design of complex intersubband-based optical devices in which complications arising from polarization fields are eliminated.

This work was supported by the NSF awards ECCS-1001431, ECCS 1253720, and DMR-1206919 and from the Defense Advanced Research Project Agency (DARPA) under Contract No. D11PC20027. Part of this research was carried out at the Center for Functional Nanomaterials, Brookhaven National Laboratory, which is supported by the U.S. Department of Energy, Office of Basic Energy Sciences, under Contract No. DE-AC02-98CH10886.

[1]P. Waltereit, O. Brandt, A. Trampert, H. T. Grahn, J. Menniger, M. Ramsteiner, M. Reiche, and K. H. Ploog, Nature **406**, 865 (2000).
[2]M. C. Schmidt, K.-C. Kim, H. Sato, N. Fellows, H. Masui, S. Nakamura, S. P. DenBaars, and J. S. Speck, Jpn. J. Appl. Phys., Part 2 **46**, L126 (2007).
[3]K.-C. Kim, M. C. Schmidt, H. Sato, F. Wu, N. Fellows, M. Saito, K. Fujito, J. S. Speck, S. Nakamura, and S. P. DenBaars, Phys. Status Solidi (RRL) **1**, 125 (2007).
[4]R. M. Farrell, P. S. Hsu, D. A. Haeger, K. Fujito, S. P. DenBaars, J. S. Speck, and S. Nakamura, Appl. Phys. Lett. **96**, 231113 (2010).
[5]Y.-D. Lin, C.-Y. Huang, M. T. Hardy, P. S. Hsu, K. Fujito, A. Chakraborty, H. Ohta, J. S. Speck, S. P. DenBaars, and S. Nakamura, Appl. Phys. Lett. **95**, 081110 (2009).
[6]R. M. Farrell, E. C. Young, F. Wu, S. P. DenBaars, and J. S. Speck, Semicond. Sci. Technol. **27**, 024001 (2012).
[7]A. Bhattacharyya, I. Friel, S. Iyer, T.-C. Chen, W. Li, J. Cabalu, Y. Fedyunin, K. F. Ludwig, Jr., T. D. Moustakas, H.-P. Maruska, D. W. Hill, J. J. Gallagher, M. C. Chou, and B. Chai, J. Cryst. Growth **251**, 487 (2003).
[8]T. Hoshi, K. Hazu, K. Ohshita, M. Kagaya, T. Onuma, K. Fujito, H. Namita, and S. F. Chichibu, Appl. Phys. Lett. **94**, 071910 (2009).
[9]E. C. Young, A. E. Romanov, C. S. Gallinat, A. Hirai, G. E. Beltz, and J. S. Speck, Appl. Phys. Lett. **96**, 041913 (2010).
[10]J. Smalc-Koziorowska, M. Sawicka, T. Remmele, C. Skierbiszewski, I. Grzegory, and M. Albrecht, Appl. Phys. Lett. **99**, 061901 (2011).
[11]B. Leung, Q. Sun, C. D Yerino, J. Han, and M. E Coltrin, Semicond. Sci. Technol. **27**, 024005 (2012).
[12]J. H. Kim, S.-M. Hwang, Y. G. Seo, K. H. Baik, and J. H. Park, Semicond. Sci. Technol. **28**, 085007 (2013).
[13]J. Jeong, J. Jang, J. Hwang, C. Jung, J. Kim, K. Lee, H. Lim, and O. Nam, J. Cryst. Growth **370**, 114 (2013).
[14]A. E. Romanov, E. C. Young, F. Wu, A. Tyagi, C. S. Gallinat, S. Nakamura, S. P. DenBaars, and J. S. Speck, J. Appl. Phys. **109**, 103522 (2011).
[15]A. Tyagi, F. Wu, E. C. Young, A. Chakraborty, H. Ohta, R. Bhat, K. Fujito, S. P. Den Baars, S. Nakamura, and J. S. Speck, Appl. Phys. Lett. **95**, 251905 (2009).
[16]R. Schuber, Y. L. Chen, C. H. Shih, T. H. Huang, P. Vincze, I. Loe, L. W. Chang, Th. Schimmel, M. M. C. Chou, and D. M. Schaadt, J. Cryst. Growth **323**, 76 (2011).
[17]K.-C. Kim, M. C. Schmidt, F. Wu, M. B. McLaurin, A. Hirai, S. Nakamura, S. P. DenBaars, and J. S. Speck, Appl. Phys. Lett. **93**, 142108 (2008).
[18]R. Liu, A. Bell, F. A. Ponce, C. Q. Chen, J. W. Yang, and M. A. Khan, Appl. Phys. Lett. **86**, 021908 (2005).
[19]T. Guühne, Z. Bougrioua, P. Vennéguès, and M. Leroux, J. Appl. Phys. **101**, 113101 (2007).
[20]F. Wu, A. Tyagi, E. C. Young, A. E. Romanov, K. Fujito, S. P. DenBaars, S. Nakamura, and J. S. Speck, J. Appl. Phys. **109**, 033505 (2011).
[21]J. Shao, L. Tang, C. Edmunds, G. Gardner, O. Malis, and M. Manfra, J. Appl. Phys. **114**, 023508 (2013).
[22]Y. Wang, A. S. Özcan, K. F. Ludwig, Jr., A. Bhattacharyya, T. D. Moustakas, L. Zhou, and D. J. Smith, Appl. Phys. Lett. **88**, 181915 (2006).
[23]G. W. Lorimer, Miner. Mag. **51**, 49 (1987).
[24]J. A. Chisholm and P. D. Bristowe, J. Phys. Condens. Matter **11**, 5057 (1999).
[25]M. Albrecht, L. Lymperakis, J. Neugebauer, J. E. Northrup, L. Kirste, M. Leroux, I. Grzegory, S. Porowski, and H. P. Strunk, Phys. Rev. B **71**, 035314 (2005).
[26]A. Bourret, C. Adelmann, B. Daudin, J.-L. Rouviere, G. Feuillet, and G. Mula, Phys. Rev. B **63**, 245307 (2001).
[27]L. Lymperakis and J. Neugebauer, Phys. Rev. B **79**, 241308(R) (2009).
[28]F. Wu, Y.-D. Lin, A. Chakraborty, H. Ohta, S. P. DenBaars, S. Nakamura, and J. S. Speck, Appl. Phys. Lett. **96**, 231912 (2010).